Progress Towards an LES Wall Model Including Unresolved Roughness

Kyle Craft[1], Andrew Redman[2], Kurt Aikens[3]
Department of Physics, Houghton College, One Willard Ave., Houghton, NY 14744
[1]kyle.craft16@houghton.edu, [2]andrew.redman17@houghton.edu, [3]kurt.aikens@houghton.edu

Abstract

Wall models used in large eddy simulations (LES) are often based on theories for hydraulically smooth walls. While this is reasonable for many applications, there are also many where the impact of surface roughness is important. A previously developed wall model has been used primarily for jet engine aeroacoustics. However, jet simulations have not accurately captured thick initial shear layers found in some experimental data. This may partly be due to nozzle wall roughness used in the experiments to promote turbulent boundary layers. As a result, the wall model is extended to include the effects of unresolved wall roughness through appropriate alterations to the log-law. The methodology is tested for incompressible flat plate boundary layers with different surface roughness. Correct trends are noted for the impact of surface roughness on the velocity profile. However, velocity deficit profiles and the Reynolds stresses do not collapse as well as expected for higher roughness. Possible reasons for the discrepancies as well as future work are presented.

Methodology

A compressible LES solver is used for the present simulations. It uses a sixth order compact finite difference scheme for spatial derivatives and the classical fourth order Runge-Kutta method for time integration. A sixth order spatial filter is used as an implicit subgrid scale model. The utilized equilibrium wall model is based on an instantaneous application of the log-law to determine the wall shear stress. This is then applied as part of an adiabatic flux boundary condition at the wall, similar to the methodology used by Kawai and Larsson [1]. For more information on the utilized methodology, see Aikens [2].

To extend the wall model to include the effects of unresolved wall roughness, simple modifications to the log law are utilized. The log law for a smooth wall is given by

$$u^+ = \frac{1}{\kappa}\ln(y^+) + B,$$

where u^+ is the wall-parallel velocity and y^+ is the wall-normal distance. Both variables are nondimensionalized as usual by using the wall shear stress. Furthermore, $\kappa = 0.41$ and $B = 5.0$. More generally, however, B is a function of the wall roughness which is often expressed in terms of k_s, an equivalent sand grain roughness. For small k_s^+, the wall is said to be "hydraulically smooth" and B is 5.0, the value for a smooth wall. For large k_s^+, however, the wall is "fully rough" for which [3]

$$B(k_s^+) = 8.5 - \frac{1}{\kappa}\ln(k_s^+).$$

In the present methodology, the hydraulically smooth and fully rough versions of the log law are smoothly combined. Therefore, for walls with unresolved roughness

$$u^+ = \frac{1}{\kappa}\ln(y^+) + \begin{cases} 5.0, & 0 \le k_s^+ \le \exp(3.5\kappa) \\ 8.5 - \frac{1}{\kappa}\ln(k_s^+), & k_s^+ > \exp(3.5\kappa) \end{cases}.$$

Algorithmically, the wall shear stress is calculated assuming a smooth wall. If $k_s^+ > \exp(3.5\kappa)$, however, the wall shear stress is recalculated using the log law for a fully rough wall.

Results

Figure 1 shows that for increasing roughness, the simulations fit the experimental data well for lower values of roughness, i.e. $k_s^+ \le 26$. The results for $k_s^+ = 16$ do not agree as well because $k_s^+ = 16$ is a transitional roughness – between what is considered hydraulically smooth and fully rough. Larger discrepancies between the simulation results and the experimental data are noted for $k_s^+ \ge 56$.

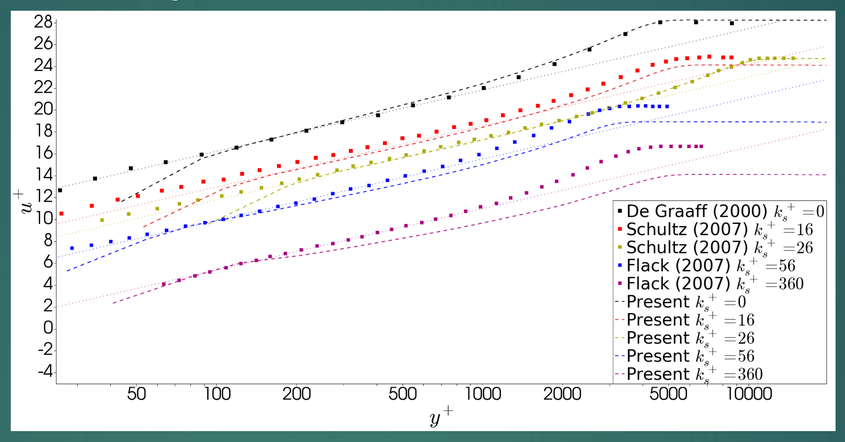

Figure 1. A plot of u^+ vs. y^+ data for varying levels of roughness compared with experimental data. The dotted lines show the combined log law for each k_s^+ value.

In figures 2 and 3, results for the different levels of roughness are expected to collapse according to Townsend's hypothesis [7], especially farther away from the wall. This is exemplified by the experimental results. Similar to the data shown in Figure 1, simulation results are closer to the experimental data for low roughness but are less accurate as the roughness increases.

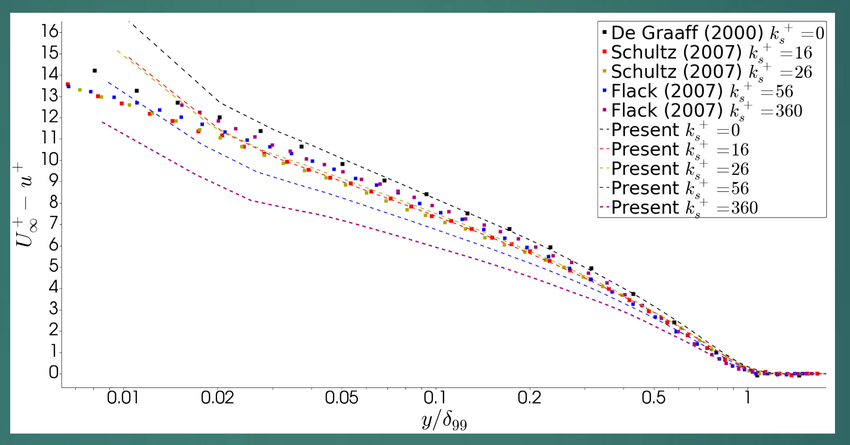

Figure 2. A plot of the velocity deficit vs. height from the wall.

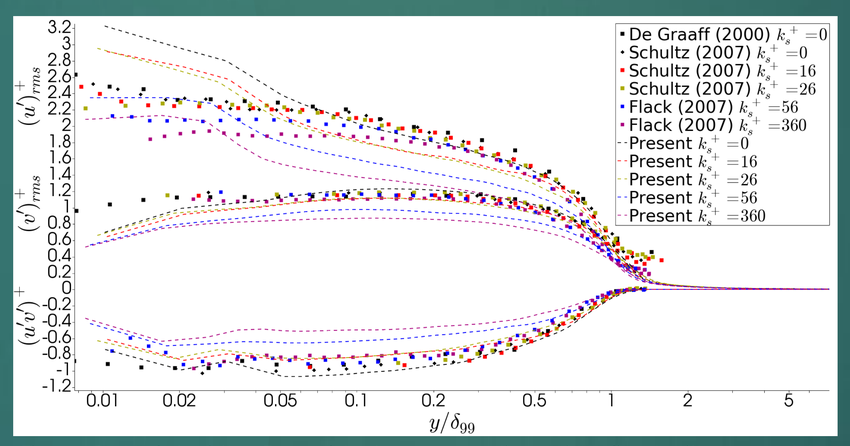

Figure 3. A plot of the Reynolds stresses nondimensionalized with respect to the friction velocity, u_τ. In the figure, u' is the streamwise Reynolds stress, v' is the wall-normal Reynolds stress, and $u'v'$ is the Reynolds shear stress.

In Figure 4 the turbulence levels are expected to increase with increasing roughness, as seen, but they do not increase as quickly as those for the experimental data. Similar trends are found for the other Reynolds stresses (not shown).

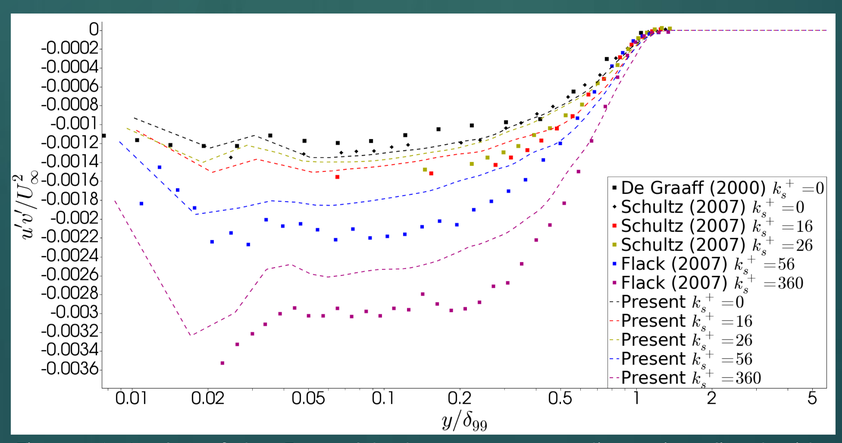

Figure 4. A plot of the Reynolds shear stress nondimensionalized with respect to the freestream velocity, U_∞.

Simulation Conditions

All simulations are performed at a freestream Mach number of 0.2 to approximate an incompressible flow. For each roughness case, a different Reynolds number is used to match that of the experimental data. The inflow Reynolds number is chosen such that the flow reaches the Reynolds number of the experimental data at $x/\delta_{99i} \approx 30$, where δ_{99i} is the inflow boundary layer thickness and x is the streamwise coordinate. This allows for flow redevelopment from the approximate turbulent inflow boundary condition and avoids effects from the sponge zone near the outflow. Additional details for the simulations are included in Table 1. The experimental data comes from De Graaff and Eaton [4], Schultz and Flack [5], and Flack et al. [6]. The simulations match the experimental Re_θ and the k_s^+ values match to within 1%.

Table 1. A comparison of the computational case details tested with their corresponding experiments.

Exp. k_s^+	Sim. k_s^+	k_s/δ_{99i}	$Re_{\delta 99i}$	δ_{99}/k_s	Re_θ
0	0	0	91,000	-	13,140
16	16.7	0.00433	94,000	307	13,800
26	26.4	0.00389	169,000	372	27,080
56	57.8	0.029	38,000	53.4	7,190
360	385	0.13	42,000	12.4	8,970

The timestep size for each case is chosen such that the maximum CFL number obtained is 0.8. All cases are run for $250\delta_{99i}/U_\infty$ time units before collecting statistics for $250\delta_{99i}/U_\infty$ time units, where U_∞ is the velocity at the edge of the boundary layer. All simulations use a domain size of (50 x 15 x 3) δ_{99i} with grid spacings $\Delta x = \Delta z = 0.042\delta_{99i}$ in the streamwise and spanwise directions respectively, and $\Delta y = 0.055\delta_{99i}$ as the wall-normal spacing at the wall. There is constant spacing from the wall to $2\delta_{99i}$, hyperbolic tangent stretching from $2\delta_{99i}$ to $5\delta_{99i}$ with a maximum stretching ratio of 4%, and constant stretching from $5\delta_{99i}$ to $15\delta_{99i}$ with a stretching ratio of 15% to dampen acoustic waves before they reach the upper boundary condition. The wall model/LES matching point is chosen as the fourth grid point off the wall. Each grid has 21 million points, uses 368 cores, and takes about 5000 core-hours to run on TACC Stampede.

Conclusions

A simple extension has been proposed for incorporating the effects of unresolved wall roughness into an existing wall model. This method excels in its simplicity but relies on the equivalent sand grain roughness which is often not known a priori. While results are less accurate for high levels of roughness, this may be due to the roughness being so large that it also affects the outer boundary layer flow and not just that near the wall. Jiménez proposes that this occurs for $\delta_{99}/k < 50$ [3]. For $k_s^+ \le 26$, this condition is not met and good results are obtained. Roughness values of $k_s^+ \ge 56$, however, are closer to this limit and inaccurate results are noted. Future work includes finding the maximum δ_{99}/k_s for which suitable results can be expected. Additional research into correlations between the roughness geometry and k_s also needs to be performed. One such correlation is proposed by Flack and Schultz [8].

References

[1] S. Kawai and J. Larsson, Phys. Fluids **24** (1), 015105 (2012).
[2] K. M. Aikens, Ph.D. thesis, Purdue University, 2014.
[3] J. Jiménez, Annu. Rev. Fluid Mech. **36**, 173 (2004).
[4] D. B. De Graaff and J. K. Eaton, J. Fluid Mech. **422**, 319 (2000).
[5] M. P. Schultz and K. A. Flack, J. Fluid Mech. **580**, 381 (2007).
[6] K. A. Flack, M. P. Schultz, and J. S. Connelly, Phys. Fluids **19** (9), 095104 (2007).
[7] A. A. Townsend, *The structure of turbulent shear flow*. (Cambridge Univ. Press, 1980).
[8] K. A. Flack and M. P. Schultz, J. Fluids Eng. **132** (4), 041203 (2010).

Acknowledgements

The authors gratefully acknowledge Gregory A. Blaisdell from Purdue University and Anastasios S. Lyrintzis from Embry-Riddle Aeronautical University for their support with utilizing their LES application. This work used the Extreme Science and Engineering Discovery Environment (XSEDE), which is supported by National Science Foundation grant number ACI-1053575. Computational resources are provided on TACC Stampede under XSEDE allocation number ENG150001.